Electronic Supplementary Information for

Melt-processing of small molecule organic photovoltaics via bulk heterojunction compatibilization

*Aiman Rahmanudin, Liang Yao, Xavier A. Jeanbourquin, Yongpeng Liu, Arvindh Sekar, Emilie Ripaud and Kevin Sivula**

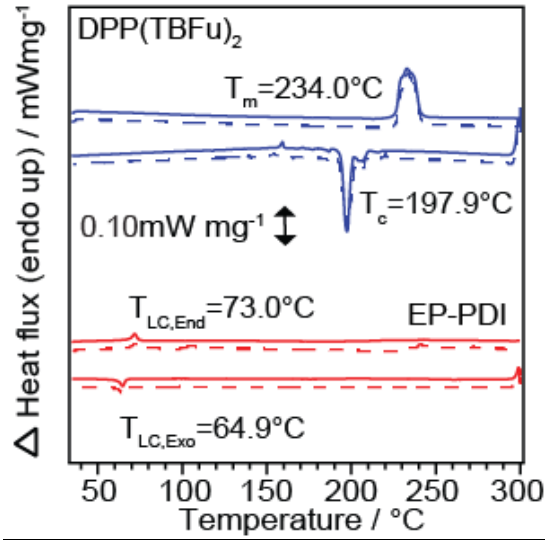

Figure S1. DSC Thermograms of the 1st (broken line) and 2nd (solid line) heating and cooling scans of $DPP(TBFu)_2$ (Blue) and EP-PDI (Red). The temperatures for melting (T_m), and crystallization (T_c) of the $DPP(TBFu)_2$, along with the endothermic and exothermic liquid crystal transitions of the EP-PDI ($T_{LC,End}$ and $T_{LC,Exo}$) are indicated. The temperatures were estimated from the peaks during the 2nd heating scan.

Table S1. Calculated endothermic and exothermic (specific) enthalpies of 1:1 BHJs of $DPP(TBFu)_2$:EP-PDI with varying MCPwt%. See experimental procedure for detailed sample preparation and measurement conditions.

MCP (%)	*Specific enthalpy (J/g)*				*Temperature (°C)*			
	Endothermic		**Exothermic**		**Endothermic**		**Exothermic**	
	$DPP(TBFu)_2$	**EP-PDI**	**$DPP(TBFu)_2$**	**EP-PDI**	**$DPP(TBFu)_2$**	**EP-PDI**	**$DPP(TBFu)_2$**	**EP-PDI**
0	20.574	2.785	20.216	3.585	230.5	73.3	208.4	59.4
10	9.074	0.852	7.61	1.20	217.6	70.2	196.2	57.7
25	7.0624	0.206	6.299	0.5285	212.1	69.6	187.4	52.6
50	5.85	0	-	-	202.4	-	-	-
75	-	-	-	-	-	-	-	-

[a] *The endothermic and exothermic (specific) enthalpies were calculated based on the integration of each phase transition using the exact mass of the component in the blend.*

[b] *The respective endothermic and exothermic temperatures were characterized by their peak temperature.*

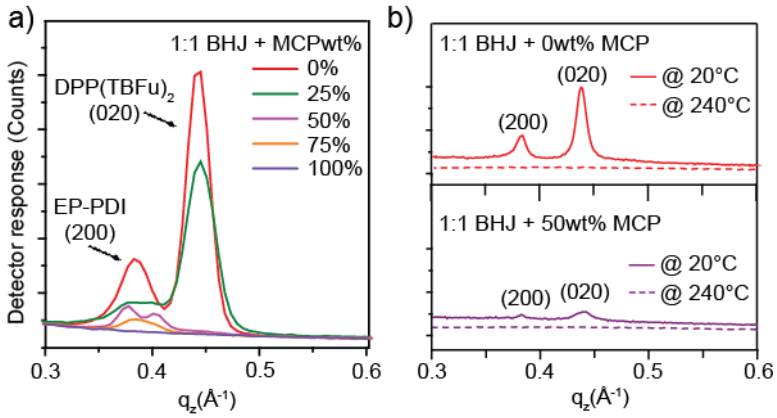

Figure S2. X-ray diffraction results. Panel (a) shows the out-of-plane grazing-incidence wide-angle X-ray scattering patterns of 1:1 BHJs with added MCP in thin films that have been treated at 240°C for 15 min and cooled over 30 min to room temperature. Panel (b) shows *in-situ* X-ray scattering patterns (Bragg-Brentano geometry) of BHJ thin films at 20 °C (solid-line) and at 240 °C (dash-line) with 0 wt% (top) and 50 wt% (bottom) of MCP.

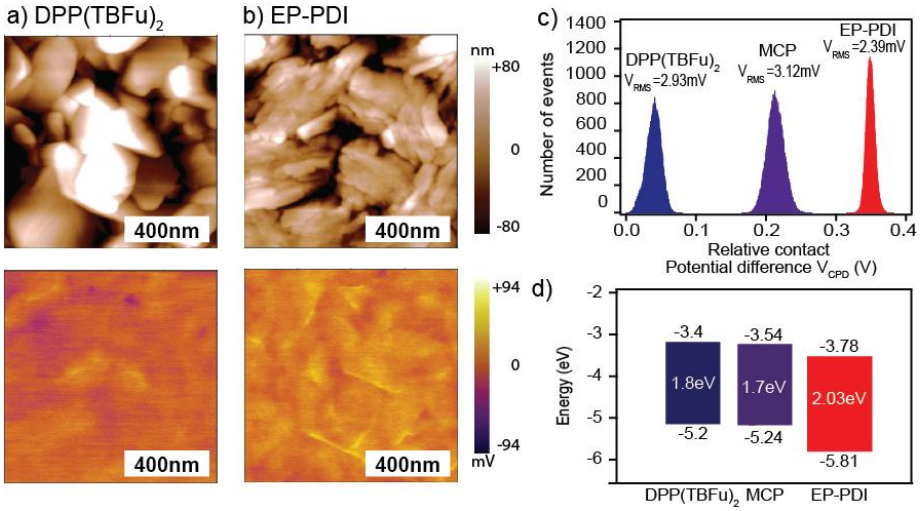

Figure S3. AFM and KPFM analysis: Height-topography and potential images of individual components a) DPP(TBFu)$_2$, b) MCP, Panel (c) shows the relative contact potential difference (V_{CPD}) histograms of the individual components d) Estimated HOMO-LUMO levels measured by the UV-Vis absorption (see Figure S9a) and cyclic voltammetry (see Figure S9b).

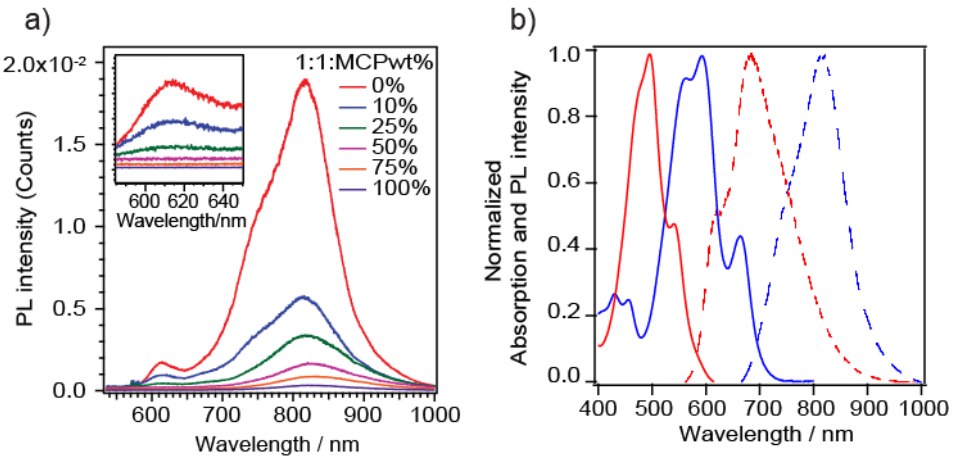

Figure S4. a) Photoluminescence emission spectra after excitation at 532 nm of melt-annealed BHJ thin films of DPP(TBFu)$_2$:EP-PDI – 1:1 with varying amount of MCP w (Inset shows zoomed spectra between 580-650 nm to indicate the emission peak for EP-PDI); b) shows the data for the pure components: DPP(TBFu)$_2$ (Blue) and EP-PDI (Red) (solid lines indicate UV-Vis absorption spectra and dotted lines indicate its PL emission).

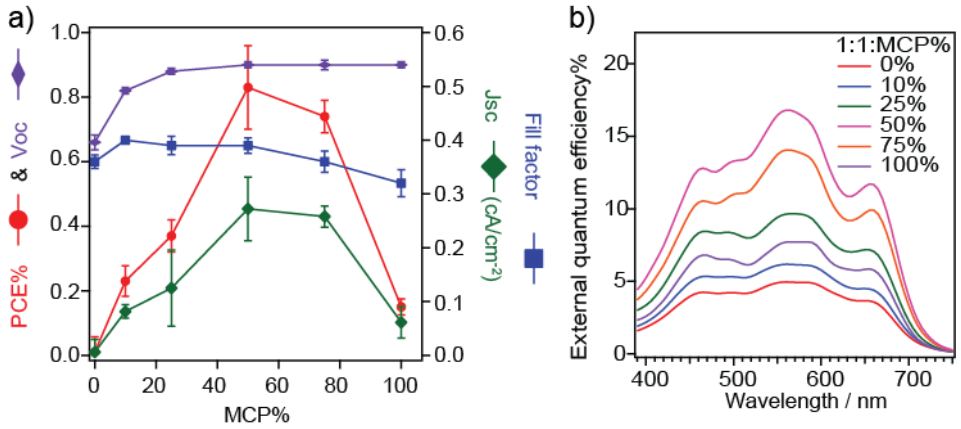

Figure S5. Summary of photovoltaic parameters of the melt-annealed devices: a) Graphical representation of PCE% (Red), open circuit voltage (Purple), short-circuit current (Green) and fill factor (Blue).

Table S2. The values of the respective device performance parameters averaged from 5 devices fabricated at each condition.

MCP (%)	*Voc (V)*	*Jsc[b] (mA/cm²)*	*FF (%)*	*PCE (%)*
0	0.66±0.023	0.23±0.024	0.36±.0013	0.010±0.047
10	0.82±0.0098	0.815±0.13	0.40±0.0047	0.23±0.050
25	0.88±0.0094	1.24±0.071	0.39±0.017	0.37±0.017
50	0.9±0.0094	2.72±0.059	0.39±0.059	0.83±0.014
75	0.9±0.015	2.58±0.020	0.36±0.0196	0.74±0.020
100	0.9±0.0095	0.614±0.029	0.32±0.029	0.116±0.025

[a] Error bars were calculated based on an average of 5 separate photovoltaic devices.

[b] Values presented in Figure S5 were converted from mA/cm² to cA/cm².

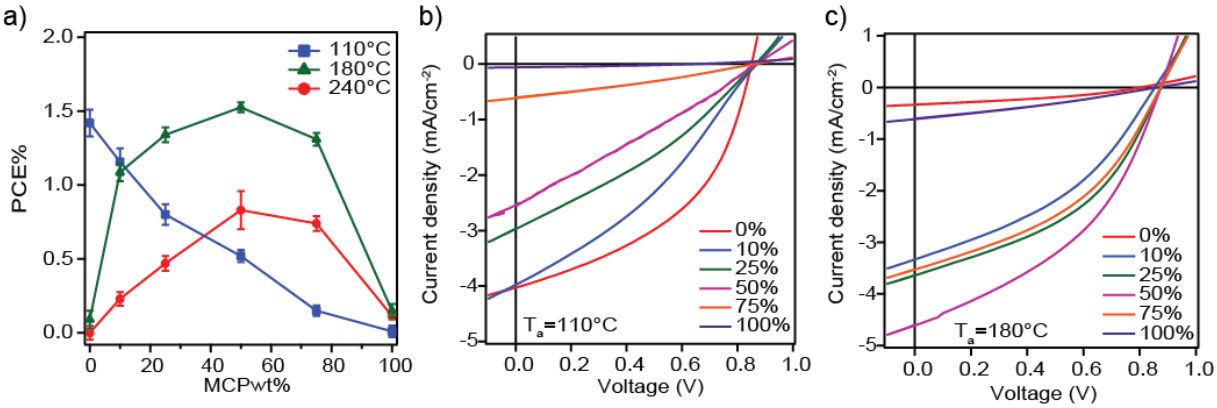

Figure S6. Photovoltaic performance of devices with 1:1 ratio of DPP(TBFu)$_2$:EP-PDI with varying amounts of MCPwt% at different annealing temperatures (BHJ cast from chloroform): a) PCE vs MCPwt% (Red 240 °C, Green – 180 °C and blue – 110 °C); Current vs voltage curves for devices at b) T_a = 110 °C b) and c) T_a = 180 °C. (see experimental procedure for detailed thin film preparation and device fabrication method).

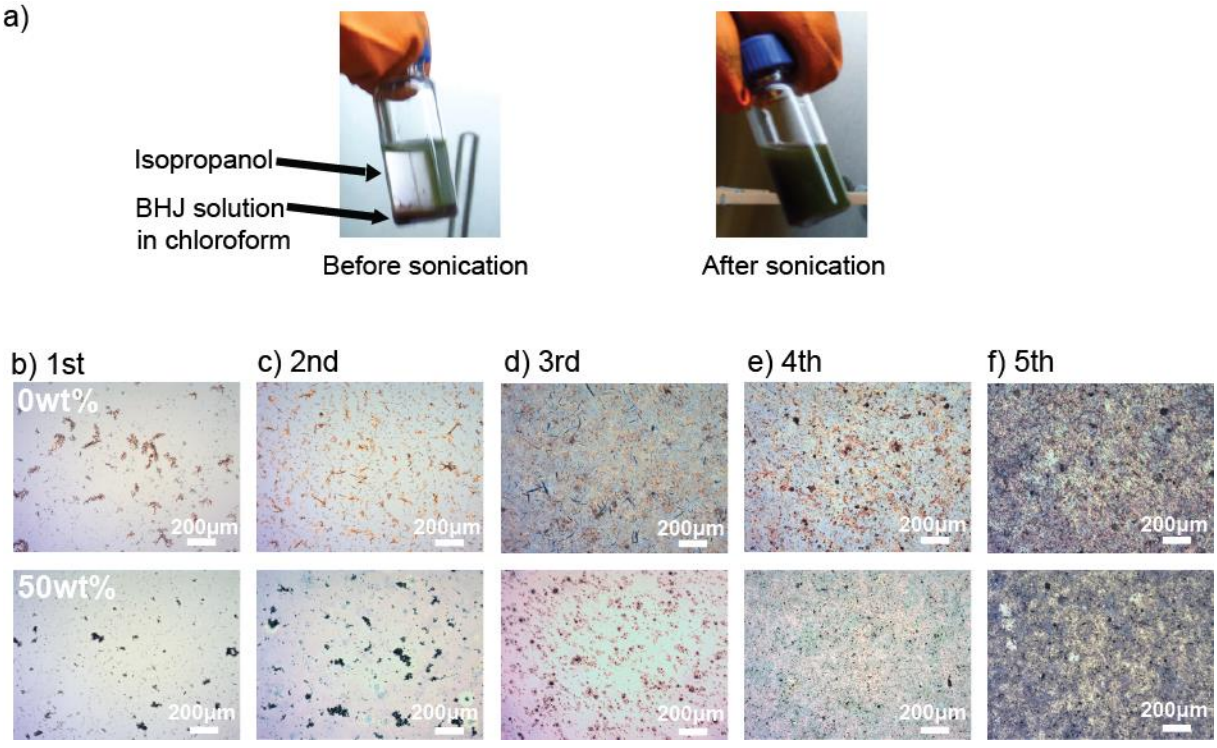

Figure S7. Solid-dispersion procedure: a) Picture of BHJ solid dispersion in IPA before and after sonication for 30 min; b-f) Optical microscope images of the sequential drop-casting of the BHJ solid dispersion with 0 and 50 wt% MCP. See experimental procedure for detailed BHJ solution and thin film preparation.

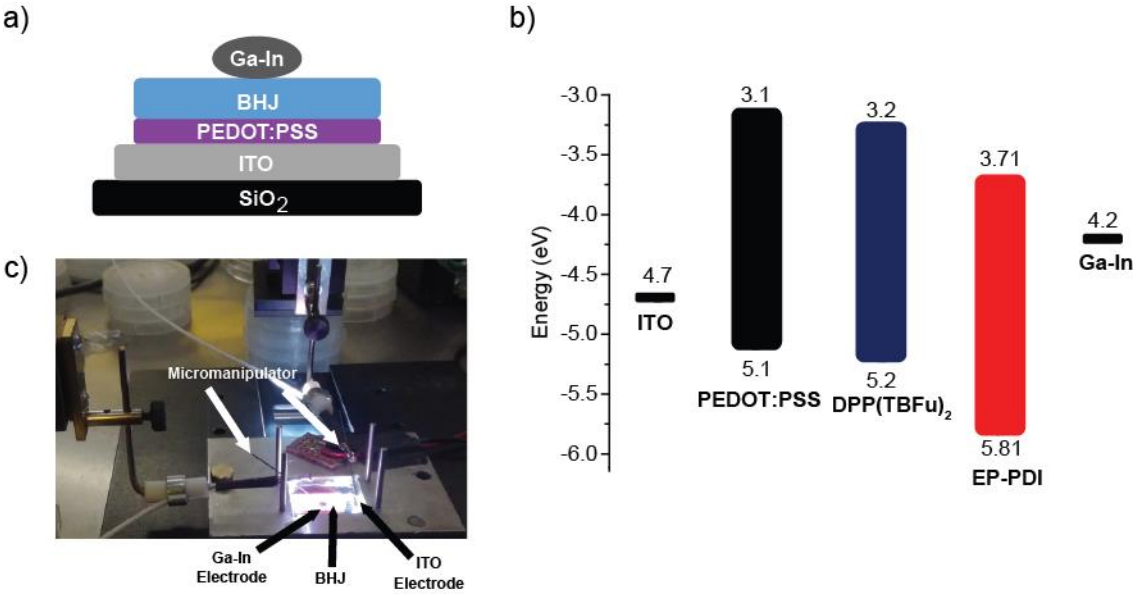

Figure S8. Solid-state melt processed photovoltaic device fabrication schematics. a)schematic of the device architecture; b) Energy Level diagram of the device configuration; c) Picture of the photovoltaic measurement set-up using two micromanipulator contacts on ITO and Ga-In electrodes. Device fabrication was based on reference literature procedures using Ga-In eutectic electrodes [S1] and see experimental procedures for detailed explanation.

Table S3. Photovoltaic parameters measured from the two dispersion cast/melt processed devices.

MCP *(%)*	*Voc* *(V)*	*Jsc*[a] *(mA/cm²)*	*FF* *(%)*	*PCE* *(%)*
0	0.256	0.0571	0.19	0.0023
10	0.448	0.874	0.272	0.11

a) Approximate active area = 1.392 cm² - The diameter of the Ga-In drop was measured using a calliper.

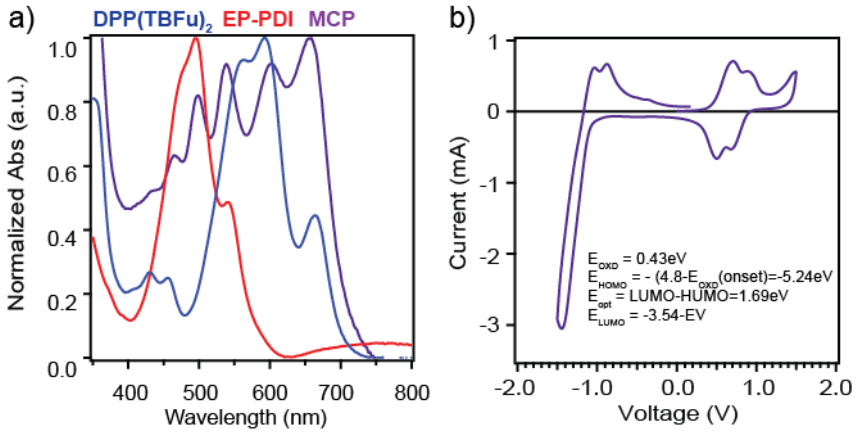

Figure S9. a) UV-vis absorption of the primary components and MCP and b) the cyclic voltammetry of MCP

Synthesis of the molecular compatibilizer (MCP)

Synthetic methods and characterization: All reagents were of commercial reagent grade (Sigma-Aldrich, Acros and Fluorochem) and were used without further purification. Toluene, Chloroform, Tetrahydrofuran (Fisher Chemical, HPLC grade) and chlorobenzene (Alfa Aesar, HPLC grade) were purified and dried on a Pure Solv-MD Solvent Purification System (Innovative Technology, Amesbury, United States) apparatus. Normal phase silica gel chromatography was performed with an Acros Organic silicon dioxide (pore size 60 Å, 40–50 µm technical grades). The (^{1}H) and (^{13}C) NMR spectra were recorded at room temperature using per-deuterated solvents as internal standards on a NMR Bruker Advance III-400 spectrometer (Bruker, Rheinstetten, Germany). Chemical shifts are given in parts per million (ppm) referenced to residual ^{1}H or ^{13}C signals in $CDCl_2$ (1H: 7.26, 13C: 77.16) and dichloromethane-d_2 (2H: 5.32, 13C:53.84). Atomatic-pressure-photoinonization-source (APPI) MS spectrum was recorded on an ESI/APCI LC-MS autopurification system with a ZQ Mass detector (Waters, Milford, United States) instrument using a positive mode. Matrix-assisted-laser-desorption/ionization time of flight (MALDI-TOF) MS spectrum was recorded on aBruker MALDI-TOF AutoFlex speed instrument using alpha-cyano-4-hydroxycinnamic acid as the matrix. Molecules used in the active layers were purified using a Biotage Isolera™ Spektra Accelerated Chromatographic Isolation System™ with a Biotage ZIP® Sphere cartridges (60 µm spherical silica) before device fabrication.

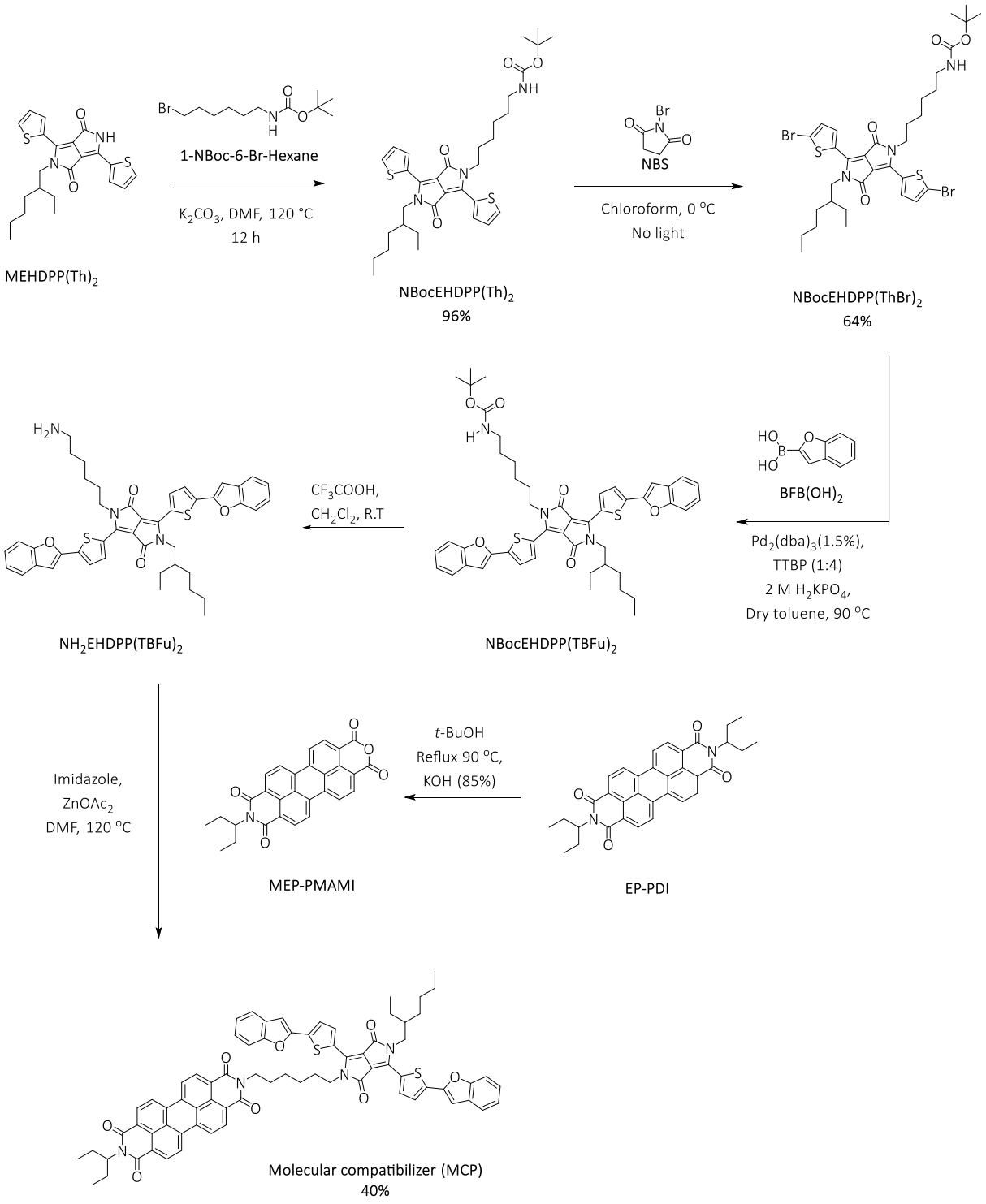

Figure S6. Full synthetic route for the Molecular compatibilizer (MCP)

Synthetic procedures: DPP(TBFu)$_2$ was synthesized according to literature procedures [S2] while EP-PDI was purchased commercially from Sigma-Aldrich. Synthesis of 2-(6-aminohexyl)-3,6- (5-(benzofuran-2-yl) thiophen-2-yl)-5-(2-ethylhexyl)-2,5- dihydropyrrolo [3,4-c] pyrrole-1,4-dione (**NH$_2$EHDPP(TBFu)$_2$**) is based on our previous report on the synthesis of a similar molecular compatibilizer [S3]. For *9-(pentan-3-yl)-1H-isochromeno[6',5',4':10,5,6]anthra[2,1,9-def]isoquinoline-1,3,8,10(9H)-tetraone* ***(MEP-PMAMI)***, dealkylation of EP-PDI was conducted via controlled hydrolysis reaction under basic

conditions of KOH (85%) with *t*-BuOH in reflux over a period of 2 h. MCP was then synthesized using a condensation reaction between a primary amine functionalized DPP(TBFu)$_2$, and a mono alkylated EP-PMAMI. Detailed synthetic steps are described below:

9-(pentan-3-yl)-1H-isochromeno[6',5',4':10,5,6]anthra[2,1,9-def]isoquinoline-1,3,8,10(9H)-tetraone (MEP-PMAMI): To a mixture of EP-PDI (6.22 g, 6.0 mmol) and *t*-BuOH (150 mL) was added 85% KOH powder (1.98 g, 30.0 mmol). The resulting mixture was refluxed for 90 °C and the conversion was monitored via TLC ($CHCl_3$/AcOH 10:1 *v/v*). After complete disappearance of the starting material (2 h), the mixture was poured slowly with stirring into Glacial Acetic acid (150 mL) and stirred for 2 h. Then 2N HCl (60 mL) was added and stirring was continued for additional 30 min until a dispersion of the precipitate is seen. This was collected by filtration, washed with water until the aqueous solution is neutral. The crude product was further purified by column chromatography on silica gel with $CHCl_3$/AcOH (10:1) to remove any starting material to obtain a dark brown solid (3.06 g, 71.4 %). ^{1}H NMR (400 MHz, Chloroform-*d*) δ 8.86 – 8.65 (m, 8H), 5.17 – 5.00 (m, 1H), 2.30 (ddd, *J* = 13.9, 9.3, 7.1 Hz, 2H), 1.98 (dt, *J* = 13.9, 6.7 Hz, 2H), 0.96 (t, *J* = 7.5 Hz,6). MS (APPI): *m/z* $[M]^+$= 461.47.

MCP: MEP-PMAMI (0.066 g, 1.43 mmol), NH_2EHDPP(TBFu)$_2$ (0.16 g, 1.43 mmol), and Zn(OAc)$_2$ (0.019 mg, 1.07 mmol) were suspended in a solution of imidazole (5 g) and DMF (10 mL). The mixture was heated overnight at 120 °C before being cooled to room temperature. Ethanol/methanol (200 mL) followed by the addition of aqueous citric acid (10%, 200 mL) was added into the mixture to precipitate the product which was removed by filtration. The crude solid was subjected to column chromatography using $CHCl_3$ as eluent and subsequently precipitated in a mixture of methanol/hexane/CH_2Cl_2 to obtain a dark purple solid (0.079 g, 40%). ^{1}H NMR (400 MHz, chloroform-*d*) δ 8.97 (dd, *J* = 15.8, 4.1 Hz, 2H), 8.60 (d, *J* = 7.9 Hz, 2H), 8.52 (d, *J* = 7.9 Hz, 2H), 8.45 (d, *J* = 8.1 Hz, 2H), 8.40 (d, *J* = 8.1 Hz, 2H), 7.51 (qd, *J* = 16.8, 15.8, 7.8 Hz, 4H), 7.41 – 7.15 (m, 6H), 7.00 (s, 2H), 5.09 (t, *J* = 8.0 Hz, 1H), 4.18 (dt, *J* = 27.4, 7.6 Hz, 4H), 4.05 (q, *J* = 11.4, 7.3 Hz, 2H), 2.30 (dp, *J* = 15.9, 7.8 Hz, 2H), 1.94 (ddt, *J* = 44.1, 15.7, 7.5 Hz,4), 1.60 (d, *J* = 10.7 Hz, 8H), 1.36 (ddd, *J* = 33.0, 14.6, 8.1 Hz, 8H), 0.95 (dt, *J* = 25.7, 7.4 Hz, 12H); ^{13}C NMR (101 MHz, $CDCl_3$) δ_C 10.56, 11.43, 14.13, 23.13, 25.04, 26.59, 26.73, 27.94, 28.51, 29.95, 30.32, 35.71, 39.25, 40.40, 42.26, 46.00, 57.77, 103.62, 111.23, 121.11, 121.18, 122.80, 122.92, 123.05, 123.44, 123.54, 125.28, 125.37, 125.61, 126.16, 128.77, 128.81, 129.16, 129.42, 129.51, 131.17, 134.21, 134.40, 136.39, 136.52, 137.88, 137.91, 154.93, 163.24; MS (MALDI-TOF): *m/z* $[M]^+$= 1186.8.

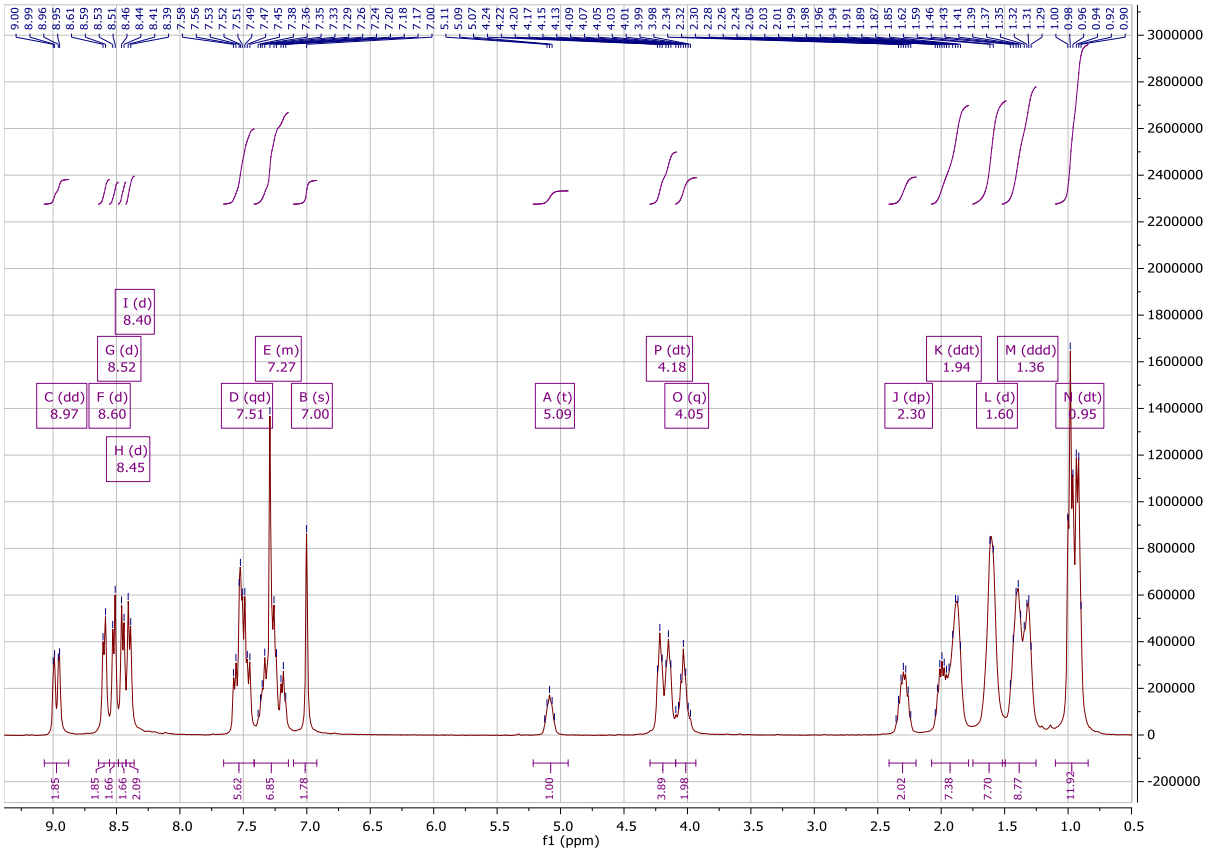

Figure S 71.[1]H NMR of MCP

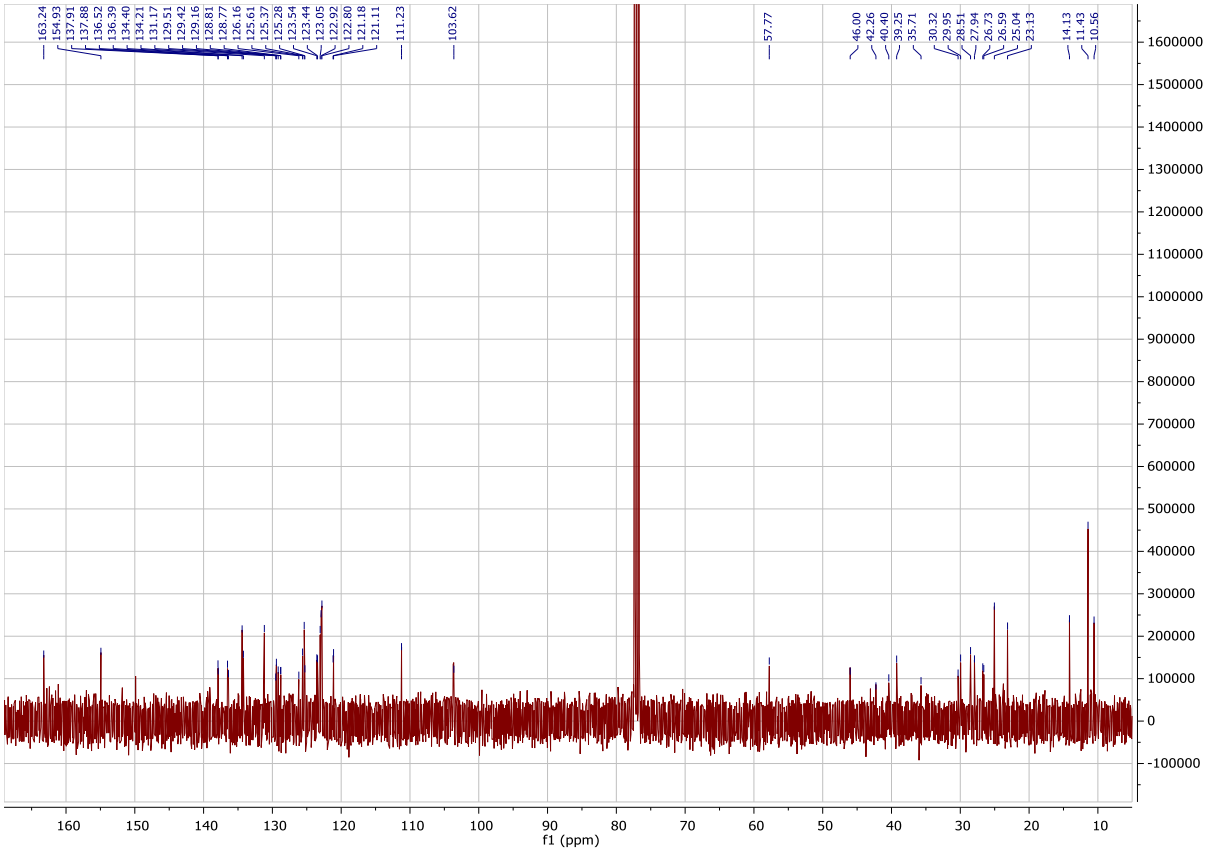

Figure S12. [1]C NMR of MCP

Supporting References

[S1] R. C. Chiechi, E. A. Weiss, M. D. Dickey, G. M. Whitesides, Angewandte Chemie International Edition 2008, 47, 142-144.

[S2] B. Walker, A. B. Tamayo, X.-D. Dang, P. Zalar, J. H. Seo, A. Garcia, M. Tantiwiwat, T.-Q. Nguyen, Adv. Funct. Mater. 2009, 19, 3063-3069.

[S3] A. Rahmanudin, X. A. Jeanbourquin, S. Hanni, A. Sekar, E. Ripaud, L. Yao, K. Sivula, J. Mater. Chem. A 2017.